Available online at www.sciencedirect.com
SCIENCE DIRECT®
PERGAMON
Control Engineering Practice 12 (2004) 665–676
CONTROL ENGINEERING PRACTICE
www.elsevier.com/locate/conengprac

System identification and controller design for dual actuated hard disk drive

T. Suthasun[a], I. Mareels[b], A. Al-Mamun[a,*]

[a] Department of Electrical and Computer Engineering, National University of Singapore, 4 Engineering Drive 3, Singapore 117576, Singapore
[b] Department of Electrical and Electronic Engineering, University of Melbourne, Vic. 3010, Australia

Received 4 July 2002; accepted 10 July 2003

Abstract

This paper describes classical system identification and control design techniques for the dual actuated servomechanism of a hard disk drive. The dual actuated servomechanism consists of a electromechanical coarse actuator and a piezo-electric micro-actuator. The coarse actuator provides the motion required to move the read–write head from one data track to another, while the micro-actuator improves the tracking performance of the servoloop. The micro-actuator also reduces the response time for small seek-length. A simple design approach is adopted in this paper. The coarse actuator loop is first designed for basic performance and stability, using estimated state feedback. The compensator for the micro-actuator is then designed to achieve better performance of the overall system. Simulation and experimental results underscore the effectiveness of the design.

Keywords: Hard disk drive; Servomechanism; Dual stage actuator; VCM actuator; Piezo-electric micro-actuator

1. Introduction

Magnetic hard disk drive storage technology continues to experience a dramatic growth in areal density (Grochowski & Hoyt, 1996). It would be very difficult to meet the demand of the high track density *Tracks-per-Inch* (TPI) with the read–write head positioning servocontroller implemented using a conventional single actuator. These actuators, typically *voice coil motors*, have large inertia limiting the responsiveness i.e. the achievable bandwidth of the servomechanism. The situation is further aggravated by the presence of lightly damped mechanical modes. Read–write heads are attached to the tip of the *suspension*, a thin beam made of stainless steel and mounted on the actuator arm. The lightly damped resonant modes are contributed by these suspensions and their couplings to the head-slider and actuator arm. Frequencies of these modes lie in the range of few kHz. This very construction of the single actuator makes it difficult to achieve a servobandwidth of 1 kHz or more. In order to achieve the desired average seek time for the high density disk drives a bandwidth larger than 1 kHz is called for. This limitation can be overcome using a dual actuated servomechanisms.

A low inertia, secondary actuator is mounted on the slow VCM actuator in a *dual-stage actuator* (DSA). The secondary actuator can move the read/write head faster and thus helps to increase the overall bandwidth. Different approaches can be considered to implement the secondary stage actuation in hard disk drives. One approach is to use a *micro-electromechanical structure* (MEMS) at the read–write head slider (Semba et al., 1999). This places the actuator very close to the point of control, i.e. the head, making it the most effective solution. The second approach, exploiting the physics of piezo-electric deformation, uses a *piezo-electric transducer* made of *Lead–Zirconium–Titanate* (PZT) alloy fabricated as an integrated part of the suspension (Evans, Griesbach, & Messner, 1999). The secondary actuator in this case is placed further away from the point of control compared to the MEMS secondary stage. This separation between the PZT actuator and read–write head is leveraged as mechanical amplification, i.e. a small deflection at the PZT can produce relatively larger deflection at the tip of the suspension

*Corresponding author. Tel.: +65-6874-2251; fax: +65-6779-1103.
E-mail address: eleaam@nus.edu.sg (A. Al-Mamun).

0967-0661/$ - see front matter © 2003 Elsevier Ltd. All rights reserved.
doi:10.1016/S0967-0661(03)00150-3

and therefore of the read/write head. The PZT micro-actuators appear to offer more attractive solution for secondary actuation. Lower acceptance of MEMS actuators is attributed to two factors—they show tortional modes at frequencies much lower than the resonant modes of the piezo-electric actuators, and mass production of reliable MEMS actuator is still a big challenge. Many research groups have designed and tested the PZT actuators for application in HDD. Research efforts have also been devoted to design high-performance and yet simple servosystem using PZT-based dual stage actuator.

For application in the head-positioning servomechanism of HDD, the piezo-electric micro-actuator is fabricated as an integrated part of the suspension. Although the length of the suspension provides mechanical amplification, the flexibility of the suspension has a detrimental effect on the dynamic characteristics of the micro-actuator manifested in the form of structural vibration. The secondary actuators have very limited range of motion, typically less than few μm. Therefore, the primary actuator is still required to effectuate motions of larger range. Bandwidth obtained using the micro-actuator is higher compared to that of the primary actuator. Therefore, the dual actuation provides a solution for implementing a servomechanism with sufficiently large bandwidth and yet the capability of long-range maneuvers.

The displacement of the read–write head slider is the combined effect of both the primary and secondary actuator. The relative displacement between the two actuators is not available as a measured signal in the DSA designed with a PZT micro-actuator for application in HDD. In other words, the DSA is a *dual-input-single-output* (DISO) system. Direct measurement of the displacement of the micro-actuator, popularly known as RPES *relative position error signal* (RPES) in the published literature, gives an advantage of independent design of controllers for the two actuators of the *dual-input-dual-output* (DIDO) system. Design and analysis presented in this paper uses a DISO model. Various methods of designing a controller for DISO system have been reported in the literature, to the extent that it is certainly time to take stock and compare various design methods. We refer the reader to Hu, Guo, Haung, and Chen (1999), Harnandez, Park, Horowitz, and Packard (1999), Hirano et al. (1998), Schroceck and Messner (2001), Horsley, Harnandez, Horowitz, Packard, and Pisano (1998), Kobayashi, Yamaguchi, and Horowitz (2000), Ding, Tomizuka, and Numasato (2000), Numasato and Tomizuka (2001), Lee, Kim, and Baek (2000), Lee, Kim, and Chung (2001), and Suh, Chung, and Lee (2001), to name but a few of the recent contributions. This paper adds to the total list of available designs, a comparison is forthcoming, and will be reported elsewhere.

This paper is organized as follows. Identification of a model of the dual-stage actuator is presented in Section 2. It describes the experimental setup used. Shortcomings of the experimental environment with respect to what would be required for a complete control design validation are reported. Open-loop model of the actuator, obtained from frequency domain analysis, is described in this section. The structure of the proposed controller and the design methodology are explained in Section 3. Advantage of the proposed structure is explained first, followed by details of the design steps. Simulation and experimental results are given in Section 4. The paper is summarized in Section 5. Plans for future works are highlighted.

2. Identification of the DSA model

The dual actuator used in our works consists of a VCM as the primary stage and a PZT micro-actuator fabricated as an integral part of the suspension as the secondary which is attached to the actuator arm using glue (Fig. 1). The VCM actuator facilitates the movement of the actuator arm cum suspension over a long range, but is slow in response due to the large inertia. Moreover, the lightly damped modes of the actuator make it difficult to achieve large bandwidth demanded by the required precision in positioning the read–write head. The PZT micro-actuator, due to its lighter mass and proximity to the head, can control the position of the read/write head with better precision, and hence is used for precise tracking of the data tracks. The displacement of the PZT actuator is restricted to a few μm only and, therefore, the motion during larger seek is dominated by the primary actuator.

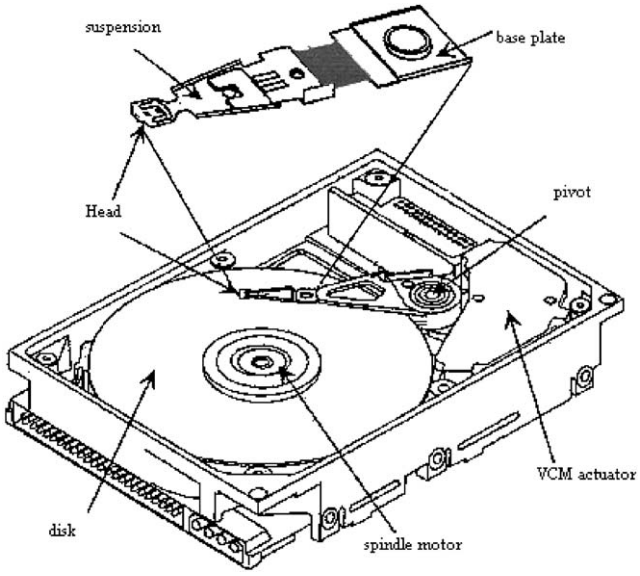

Fig. 1. Hard disk drive.

The feedback signal for the head-positioning servo-mechanism in a practical HDD is extracted from information sensed by the magnetic read-head. Position information is encoded on the tracks using pre-written spatial magnetic patterns. No such magnetic pattern and the associated demodulator circuit are available in the setup used in our experiments and the displacement of the read–write head is measured using a *laser Doppler vibrometer* (LDV). To make the observations realistic, the laser beam is shone on the slider on which the read–write head is fabricated. Same approach is used for both identification experiment and implementation of controller.

2.1. Frequency domain identification

System identification using frequency domain data gained lot of attention in the literature (Pintelon, Guillaume, Rolain, Schoukens, & Vanhamme, 1994) in the recent past. Frequency response data can easily be obtained by applying a swept sine input and collecting the input–output measurements over a desired range of frequencies. The signal-to-noise ratio can be adjusted (averaging over a longer period) in these experiments so as to ensure high fidelity measurements. A transfer function model is identified using nonlinear least-squares method (Schoukens & Pintelon, 1991), which minimizes the error function

$$\sum_{k=1}^{N}\left\|\frac{B(j\omega_k)}{A(j\omega_k)}-G(\omega_k)\right\|^2, \tag{1}$$

where, $B(s)/A(s)$ and $G(\omega_k)$ are the identified transfer function model of the plant and the frequency response measured at N different frequencies, respectively. The orders of the polynomials $A(s)$ and $B(s)$ are selected to obtain a good fit in the range of frequencies of interest.

2.2. Experimental setup

The experiments, for both identification and controller implementation mentioned in this paper, are performed using the setup shown in Fig. 2. It includes a Polytec LDV (OFN- 3001), Stanford spectral analyzer (SRT 785), a piezo-amplifier module (EPA 104), and a VCM driver. The top cover of the HDD is removed to let the LDV laser beam reach the slider. The spectrum analyzer generates the excitation signal (swept sine) for identification experiment. The excitation signal and the measured displacement signal from the LDV are fed to two input channels of the analyzer. The analyzer produces the frequency response data, and the result is saved for further processing by the frequency domain identification toolbox of $MATLAB^{TM}$ (Kollar, 1994).

2.3. Identification results

Separate experiments are carried out to get the frequency response data for each input of the DSA. The response of the primary actuator is measured in the frequency range 100–8 KHz. The input to the PZT actuator is set to zero during this stage of measurement to ensure that the secondary actuator is not excited. The response of the secondary actuator is measured in the frequency range 100 Hz–20 kHz. The VCM actuator is biased with a constant current during this set of measurements to overcome the effect of bias force exerted on the VCM actuator by the flex cable. The measurement results are presented in Figs. 3–6.

The responses from the voice coil motor, Figs. 3 and 4, with the piezo-electric actuator locked, can be modeled as a double integrator plus several lightly damped resonant modes at high frequencies. The double

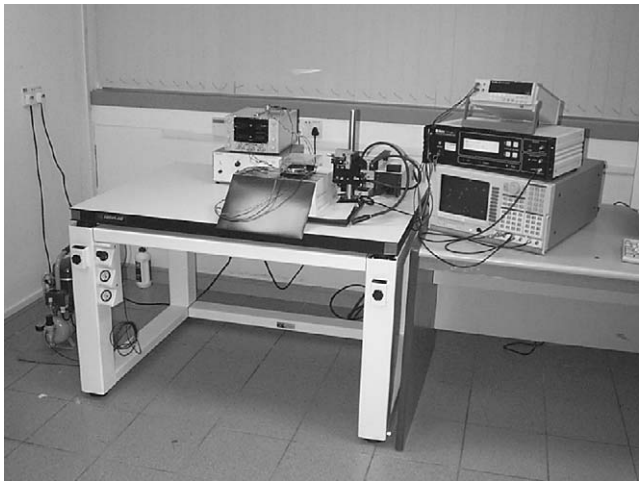

Fig. 2. Experimental setup.

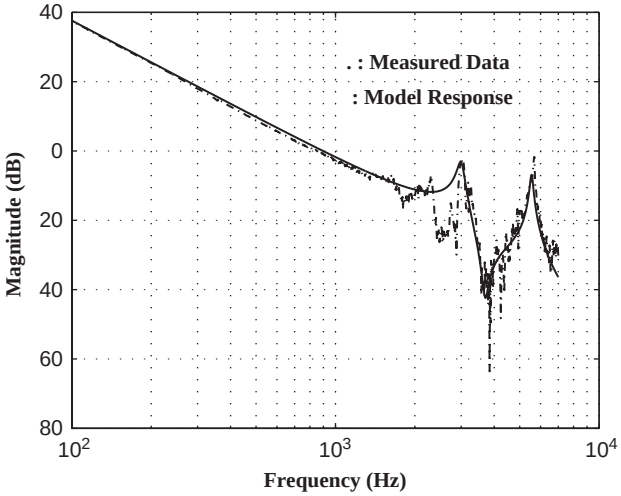

Fig. 3. Frequency response(magnitude) of the VCM actuator.

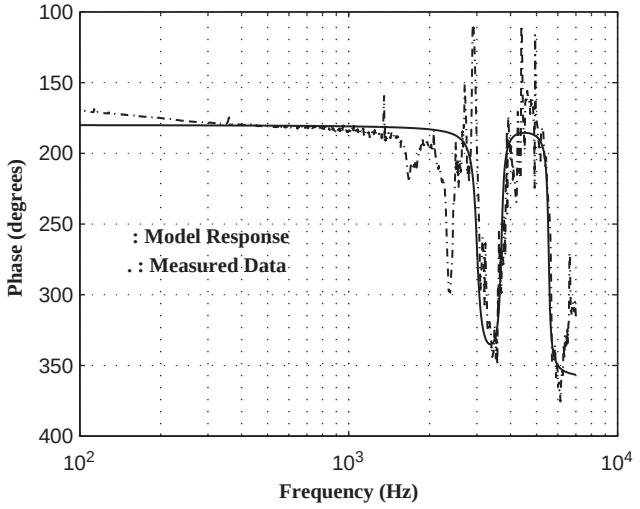

Fig. 4. Frequency response (phase) of the VCM actuator.

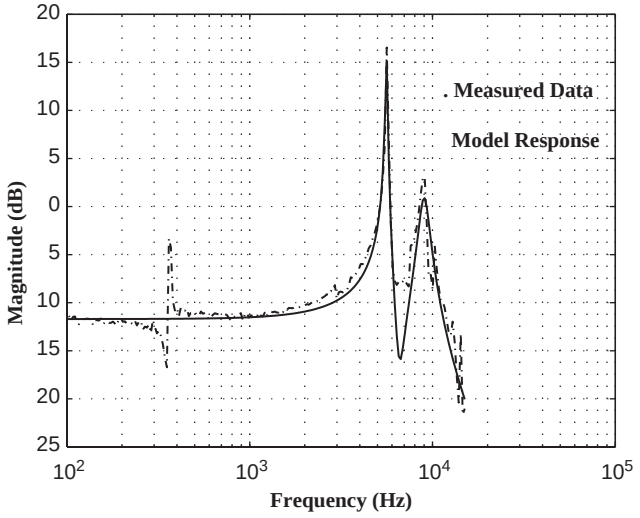

Fig. 5. Frequency response (magnitude) of the PZT actuator.

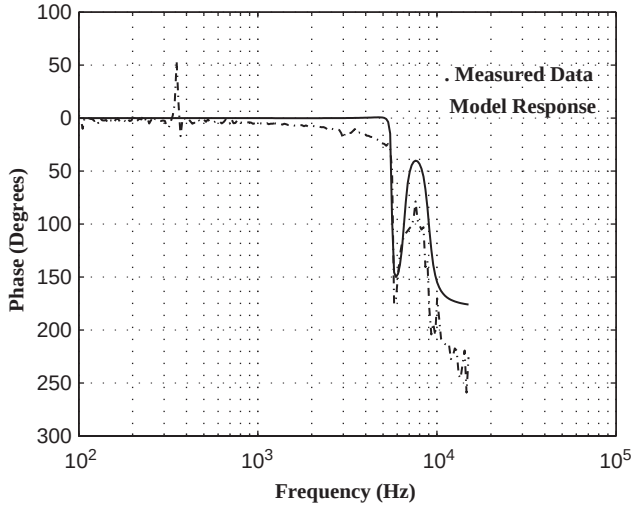

Fig. 6. Frequency response (phase) of the PZT actuator.

integrator approximation is valid for the frequency range upto about 1 kHz, with main resonance appearing above 3 kHz. Identified model of the VCM actuator is

$$G_v(s) = \frac{K_v}{s^2} H_{d1}(s) H_{d2}(s) H_{d3}(s). \quad (2)$$

The rigid body dynamics of the VCM actuator is described by the double-integrator K_v/s^2. The transfer functions $H_{d1}(s)$, $H_{d2}(s)$ and $H_{d3}(s)$ represent the dynamics of three pairs of dominant lightly damped poles and zeros clearly visible in the measured frequency response. These transfer functions are

$$H_{d1}(s) = \frac{\omega_{vp1}^2}{s^2 + 2\zeta_{vp1}\omega_{vp1}s + \omega_{vp1}^2},$$

$$H_{d2}(s) = \frac{s^2 + 2\zeta_{vz1}\omega_{vz1}s + \omega_{vz1}^2}{\omega_{vz1}^2},$$

$$H_{d3}(s) = \frac{\omega_{vp2}^2}{s^2 + 2\zeta_{vp2}\omega_{vp2}s + \omega_{vp2}^2}. \quad (3)$$

The parameters of the identified models are shown in Table 1. A simple double integrator model is used to design the feedback controller for the VCM. For simulation of the closed-loop system and for evaluation studies we use a plant model given by Eq. (2).

The response of the micro-actuator shows constant gain for a wide range of frequencies (Fig. 5), and lightly damped resonant behavior at higher frequencies. The parameters of the model containing two pairs of lightly damped complex poles and a pair of lightly damped zeros (Eq. (4)), estimated from the experimental frequency response data, are shown in Table 2. The

Table 1
Identified parameters of the VCM actuator

Parameter	Symbol	Value
Acceleration constant	K_v	3×10^7 Hz^{-2}
First pole freq	ω_{vp1}	18850 rad/s
Second pole freq	ω_{vp2}	34840 rad/s
First zero freq	ω_{vz1}	24540 rad/s
First pole damping	ζ_{vp1}	0.03
Second pole damping	ζ_{vp2}	0.014
First zero damping	ζ_{vz1}	0.02

Table 2
Identified parameters of the micro-actuator

Parameter	Symbol	Value
DC gain	K_m	0.25 Hz^{-2}
First pole freq	ω_{mp1}	35180 rad/s
Second pole freq	ω_{mp2}	56550 rad/s
First zero freq	ω_{mz1}	41220 rad/s
First pole damping	ζ_{mp1}	0.010
Second pole damping	ζ_{mp2}	0.065
First zero damping	ζ_{mz1}	0.055

simulated response of the identified model is shown using solid line in Figs. 5 and 6. The model is reasonably accurate and reliable up to about 15 kHz. In the simulation studies, we vary the frequencies of the main resonances around their nominal values by 20% to test the robustness of the controller.

$$G_m(s) = \frac{K_m\omega_{mp1}^2}{(s^2 + 2\zeta_{mp1}\omega_{mp1}s + \omega_{mp1}^2)}\frac{\omega_{mp2}^2}{\omega_{mz1}^2} \times \frac{(s^2 + 2\zeta_{mz1}\omega_{mz1}s + \omega_{mz1}^2)}{(s^2 + 2\zeta_{mp2}\omega_{mp2}s + \omega_{mp2}^2)}. \quad (4)$$

Remark 1. The measured frequency response relates an input signal measured in volts to an output signal measured in volts. So the transfer functions are unitless. The output signal can be converted into displacement unit using the scaling factor 2 μm/V.

Remark 2. The transfer functions G_v and G_m were obtained using the function 'elisml' in frequency domain identification toolbox of Matlab™. The frequency measurement data can be obtained from the authors upon request.

Remark 3. It is observed from the frequency response data that the frequency of the second resonant pole of the G_v is very close to the first resonant pole of the G_m. Modes at this frequency are thus unobservable from the available input (u_v, u_m) and output $(y = G_v u_v + G_m u_m)$.

3. Controller design

The design targets for the closed-loop system are qualitatively given as:

(1) to move the actuator fast from one track to another, and
(2) to maintain the read–write head on the center of the track with minimum variance in presence of various disturbances.

Input bias of the VCM actuator, variations in the ideally expected circular data tracks, eccentricity of disk motion, external shock and vibration, etc. are the major sources of disturbances acting on the servomechanism. The bias force is exerted by the flex cable that supports the conductors carrying signals between the heads and printed circuit board of the HDD, and must be compensated by the VCM compensator. The spectrum of the disturbances due the variations in data tracks and eccentricity in the rotation of disks is related to the angular speed of the spindle motor. With increasing spindle speed which is desirable for faster data transfer the spectrum of this disturbance moves towards high frequency and, as a result, extends beyond the achievable bandwidth of the VCM actuator. The low inertia micro-actuator is used to reject such disturbances. The actuators, both VCM and PZT, are mass-produced components and their dynamic characteristics vary from actuator to actuator. They also vary due to wear and tear, and because of changes in operating conditions. The designed controller must be robust against any variation in the actuator dynamics. The variations in the resonant frequencies of the actuators can be as high as 20% of their nominal values, and therefore become more critical than the variations in inertia.

The displacement of the read/write head during long seek is dominated by the VCM actuator. But the rejection of high-frequency disturbance and very short seek can be and should be executed using the micro-actuator. Overall advantage of the dual-stage system lies in a higher disturbance rejection capability, somewhat faster average seek time for most of the track seeking operations, and significant improvement for small track seek tasks. No optimization is performed in our design, and in general we follow rather standard design procedures e.g., those given in Morarai and Zafriou (1989) and Franklin, Powell, and Workman (1997).

Many authors treat the problem of designing controller for DISO plant as a special case of *multi-input multi-output* (MIMO) design, and use standard tools for MIMO design, such as the LQG/LTR design proposed in Hu et al. (1999), H_∞ and μ-synthesis in Harnandez et al. (1999), etc. These techniques ensure robust stability but usually produce a controller of high order, which is not so desirable from implementation's point of view. T. Hirano et al. use sequential SISO design assuming that no interaction exists between the VCM loop and the micro-actuator loop, and call this approach the *master–slave* design (Hirano et al. 1998). The problem associated with the master–slave design is overcome by Messner and co-authors using the so-called PQ method in Schroceck and Messner (2001). This method deduce directly the interference between the two single loops. Unfortunately, it ignores the issue of the stability in case of a micro-actuator failure. The stability of the VCM loop is required to ensure proper operation of the HDD servomechanism even in the event of such failure. The method presented in this paper emphasizes on the stability of the individual loops and yet uses a controller of much lower order than those obtained using conventional MIMO techniques. Simplicity in design without loss of performance is the main contribution of the proposed controller. It shows that simple physical considerations rather than brute force optimization can achieve a lot in servo design.

The desire to adequately suppress the 5.6 kHz resonance in the micro-actuator and the eccentricity disturbances leads us to select 20 kHz sampling frequency.

The designers of HDD servocontroller are often not at liberty to choose the sampling frequency arbitrarily, and the choice is determined by the tradeoff between storage capacity and servoperformance (Mamun, Lee, & Tay, 2001). This paper ignores that constraints while selecting the sampling frequency. Multi-rate controller is a realistic option to achieve good servo-performance in spite of restrictions on the sampling frequency. The bandwidth expected from the micro-actuator demands for high sampling rate. Also it is the micro-actuator that needs to suppress the 5.6 kHz resonance. The VCM, on the other hand, is not being required to achieve similar responses and its controller can be realized using a lower sampling rate. In the future, a dual sampling rate regime will be considered with lower rate for sampling the output signal and updating the VCM input, but a higher update rate for the micro-actuator input.

3.1. VCM controller

The double-integrator model of the VCM matches well with the experimental observations in the frequency range upto about 1 kHz. The first resonance of significant magnitude appears at around 3 kHz. The nominal model used to design the controller for the VCM actuator is

$$G_{vcm,nom}(s) = \frac{K_v}{s^2}. \tag{5}$$

For the frequency response data shown in Section 2.3, the acceleration constant of the double integrator model $K_v = 3 \times 10^7$.

We choose to implement a PD control, the obvious candidate for the double integrator model, using feedback of observed states. The state space representation of the double integrator model is

$$\frac{\mathrm{d}x}{\mathrm{d}t} = \begin{pmatrix} 0 & 1 \\ 0 & 0 \end{pmatrix} x + \begin{pmatrix} 0 \\ 3 \times 10^7 \end{pmatrix} u_v, \quad y_v = \begin{pmatrix} 1 & 0 \end{pmatrix} x \tag{6}$$

with $u_v(t)$ and $y_v(t)$ as the input and output of the VCM. The state vector $x = \begin{pmatrix} x_1 & x_2 \end{pmatrix}^{\mathrm{T}}$ includes the position (x_1) and velocity (x_2) of the tip of the actuator arm caused by VCM's motion. The discrete-time nominal model of the VCM actuator for 20 kHz sampling frequency and a zero-order hold is

$$x(k+1) = \begin{pmatrix} 0 & 5 \times 10^{-5} \\ 0 & 1 \end{pmatrix} x(k) + \begin{pmatrix} 0.0375 \\ 1500 \end{pmatrix} u_v(k),$$

$$y_v(k) = \begin{pmatrix} 1 & 0 \end{pmatrix} x(k). \tag{7}$$

Integral control is a possible solution for tackling the problem of input bias. But this limits the achievable bandwidth. We, therefore, estimate the disturbance using a bias estimator and compensate it directly (Franklin et al., 1997). Treating the input disturbance as a new state (x_3), we define the augmented state vector $x_a = \begin{pmatrix} x_1 & x_2 & x_3 \end{pmatrix}^{\mathrm{T}}$. Assuming the bias input to be constant, the discrete state–space model of the augmented system is

$$x_a(k+1) = A_e x_a(k) + B_e u_v(k),$$

$$y_v(k) = C_e x_a(k), \tag{8}$$

where

$$Ae = \begin{pmatrix} 1 & 5 \times 10^{-5} & 3.75 \times 10^{-2} \\ 0 & 1 & 1500 \\ 0 & 0 & 1 \end{pmatrix},$$

$$B_e = \begin{pmatrix} 3.75 \times 10^{-2} \\ 1500 \\ 0 \end{pmatrix}, C_e = \begin{pmatrix} 1 & 0 & 0 \end{pmatrix}.$$

The states of the primary actuator are estimated using the prediction observer

$$\bar{x}(k+1) = A_e \bar{x}(k) + B_e u_v(k) + L(y_v(k) - C_e \bar{x}(k)), \tag{9}$$

where L is the observer gain and $\bar{x}$ is the estimate of the actuator state vector. The augmented system is observable but not controllable and hence the input bias, though estimated, cannot be controlled using feedback. The effect of the bias is canceled by subtracting its estimated value directly from the VCM input

$$u_v(k) = -K_1 \bar{x}_1(k) - K_2 \bar{x}_2(k) - \bar{x}_3(k). \tag{10}$$

Unfortunately the output of the VCM actuator (y_v), used in the observer of Eq. (9), cannot be measured. The measured output is the sum of the displacements y_v and y_m effectuated by the VCM and micro-actuator, respectively. One can implement a controller using full order observer for the DISO model of the dual-stage actuator (Lee et al., 2000). Given the nominal models for both actuators, it requires an observer with nine states—two associated with the VCM one for estimating the input bias, and six associated with the micro-actuator (it may be mentioned that we neglect the resonances of the coarse actuator during the design, but they are included in the plant model for simulation studies). The dynamics of the micro-actuator is faster than that of the desired VCM loop response and the PZT can be modeled as a simple gain for most of the range of frequencies where VCM plays the dominant role. These features can be exploited to get a fairly accurate estimate of the VCM output (y_v) by subtracting an estimated output of the micro-actuator from the measured displacement. This scheme is shown in Fig. 7 including a model of the PZT actuator that generates an estimate ($\bar{y}_m$) of micro-actuator displacement (y_m). The

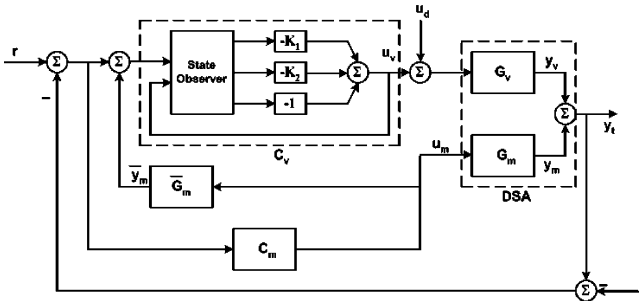

Fig. 7. Controller structure.

estimator equation of Eq. (9) is modified as

$$\bar{x}(k+1) = A_e\bar{x}(k) + B_e u_v(k) + L(y_t(k) - \bar{y}_m(k) - C_e\bar{x}(k)). \quad (11)$$

The unavoidable modeling errors of the PZT actuator contribute towards the estimation error. But this approach allows us to design a much simpler and faster observer. The (partial) observer has three states and can be about three times faster than a full nine state observer. As acquisition time is critically more important than accuracy (we have 5% tolerance during tracking) we prefer this strategy.

Because of the significant variation in frequency and damping of the suspension resonance at 3 kHz, we want to make the gain stable at this frequency. The resonant peak at 3 kHz is approximately 20 dB higher than the gain of the nominal double integrator model at that frequency. We must ensure more than 20 dB attenuation of the closed-loop frequency response (with VCM only) at 3 kHz. This is one of the design specifications for the VCM loop. A third-order controller results in if state feedback with augmented state observer is used. So we expect a closed loop with five poles and two zeros. The zeros are to be at low frequency to provide the required phase margin. A slope of -60 dB/decade, equivalent to -18 dB/octave slope, in the magnitude of the closed-loop frequency response is expected outside the bandwidth. If we achieve -3 dB bandwidth of the closed loop at 1.5 kHz, the attenuation at one octave higher frequency (3 kHz) will be -21 dB. The open-loop cross-over frequency is expected at approximately half of this frequency, i.e. 750 Hz.

It is clear that the introduction of the estimated micro-actuator output into the VCM branch, as suggested in the proposed architecture, alters the open-loop characteristics of the VCM branch. Careful observation of the control architecture shown in Fig. 7 suggests that the resultant open-loop transfer function of the VCM branch is

$$G_{OL,vcm} = (1 + C_m\bar{G}_m)C_v G_v, \quad (12)$$

where, C_m is the controller for the micro-actuator, $\bar{G}_m$ is the model of the micro-actuator, C_v is the controller for VCM using observed state, and G_v is the transfer function of the VCM. The compensator (C_m) for the PZT is designed to cancel resonant modes of the micro-actuator, details of this design is discussed in the next subsection. Under ideal assumption we can take C_m as a gain, at least for the frequencies where VCM loop is dominant. If we take $\bar{G}_m = K_m$, then the effect of $1 + C_m\bar{G}_m$ on the $G_{OL,vcm}$ is a vertical shift in the magnitude plot. If we choose the DC gain of the PZT compensator equal to the inverse of the DC gain of the micro-actuator, the magnitude of $G_{OL,vcm}$ is shifted upward by approximately 6 dB at and around the gain cross-over frequency. This effectively alters the cross-over frequency and the gain and phase margins of the VCM branch with state feedback. Keeping this in mind we specify the requirements for the margins higher than that is otherwise considered good, and select the cross-over frequency lower than 750 Hz. Our specifications for the VCM controller is therefore set at 500 Hz cross-over frequency, 10 dB of gain margin, and 35° of phase margin.

Pole-placement technique using Ackerman's formula is used to find the state feedback gain (K) and observer gain (L). But all the desired frequency domain specifications may not be satisfied by the selected poles. A simple search method, such as the *random neighborhood search* described in Franklin et al. (1997), can be used to fine tune the gains K and L so that the design specifications are met. Since the optimization of the controller is not the primary concern of this paper, we use trial-and-error approach to find the suitable gains $K = \begin{pmatrix} 0.22 & 1.5 \times 10^{-4} \end{pmatrix}$ and $L_c = \begin{pmatrix} 1.2 & 8000 & 0.55 \end{pmatrix}^{\mathrm{T}}$. Open-loop frequency responses of the VCM (with and without resonant modes) are shown in Figs. 8 and 9. Resultant cross-over frequency, gain and phase margins are tabulated in Table 3.

3.2. Micro-actuator controller

We compensate for the resonance in the micro-actuator through a robust feedforward compensator by providing a number of well-placed zeros in the range of frequencies around the resonant modes. This anti-vibration feedforward controller must be robust with respect to 20% variations in the frequencies of PZT resonance modes. As worked out in Singer (1989) this is entirely feasible. We exploit speed of the fast micro-actuator by using it in virtually open-loop mode and ensure that the VCM is used for what it is best: removing steady-state errors and gross motion. The micro-actuator is used to provide quick transient and disturbance rejection. It may be mentioned that no integrator is included in the micro-actuator compensator so that saturation of the micro-actuator during track

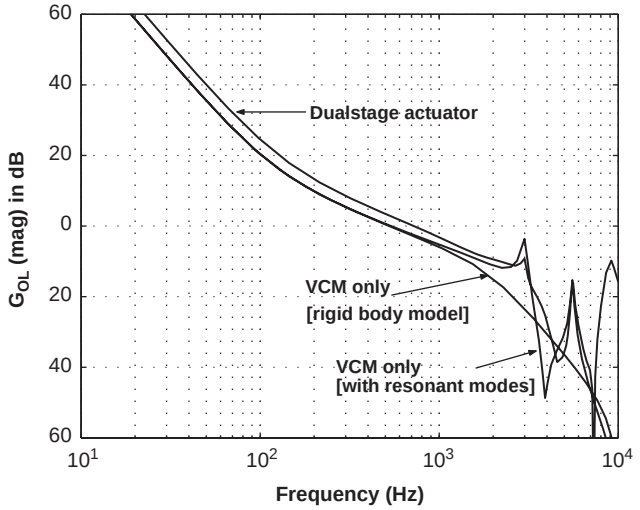

Fig. 8. Open-loop frequency response (gain).

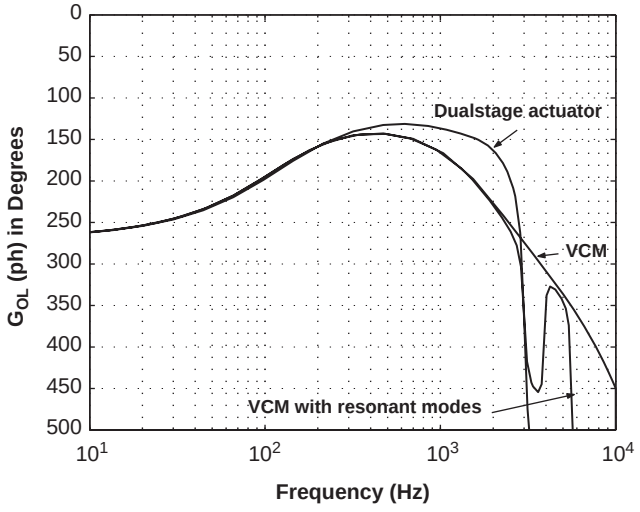

Fig. 9. Open-loop frequency response (phase).

Table 3
Design results

Description	Symbol	Value
Sampling interval	T_S	50 μs
Open loop (Stand alone VCM rigid body)		
Cross-over frequency	$f_{cv,rigid}$	526 Hz
Gain margin	$G_{mv,rigid}$	8.22 dB
Phase margin	$P_{mv,rigid}$	35.43°
Open loop (Stand alone VCM with resonant modes)		
Cross-over frequency	f_{cv}	538 Hz
Gain margin	G_{mv}	6.90 dB
Phase margin	P_{mv}	34.89°
Open loop with dual-stage actuator		
Cross-over frequency	f_{cd}	720 Hz
Gain margin	G_{md}	10.30 dB
Phase margin	P_{md}	47.58°

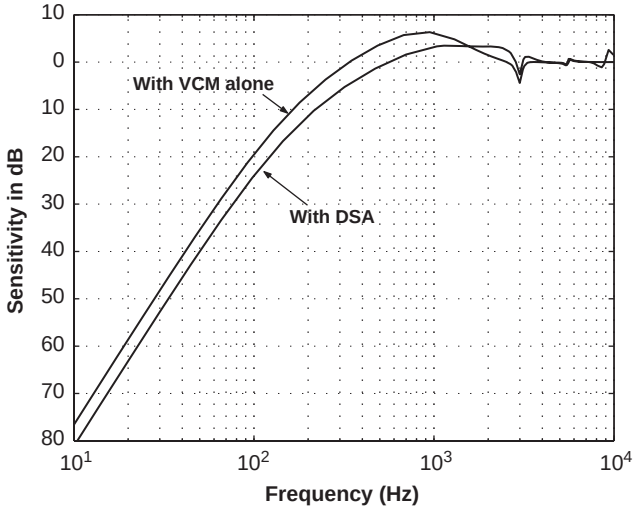

Fig. 10. Sensitivity.

following is prevented. The compensator (C_m in Fig. 7) for the micro-actuator is implemented using the FIR filter

$$C_m(z^{-1}) = 0.22(1 + 0.37z^{-1} + 0.965z^{-2}) \times (1 + 1.28z^{-1} + 0.955z^{-2}) \times (1 - 0.32z^{-1} + 0.97z^{-2}). \quad (13)$$

Because the micro-actuator is approximately five times faster than the VCM actuator we allow the micro-actuator to act on the same position error as fed to the primary actuator. This has a consequence that the fast micro-actuator will quickly saturate for large changes in the position reference, and only when the VCM actuator has brought the error down to within the operational range of the micro-actuator good tracking will be ensured. Such control mimics qualitatively time optimal control. Positioning of the micro-actuator in the center of its operational range is also optimal from a disturbance rejection point of view. Figs. 8 and 9 show the simulated open-loop frequency response of the dual-stage system. The cross-over frequency, gain margin, and phase margin for the dual-stage are tabulated in Table 3. The sensitivity or error transfer functions $S_{vcm}(j\omega)$ with VCM alone and $S_{dsa}(j\omega)$ with DSA, respectively, are shown in Fig. 10. It is obvious that the dual-stage actuator provides better bandwidth and, hence, better tracking.

4. Results

Effectiveness of the designed controller is verified using both simulation and experiment. Although the controllers are designed using nominal models of the

two actuators, high-order plant model including all the significant resonant modes are used for simulating the dynamics of the plant. Robustness of the controller is verified through simulation only. Experimental implementation shows only the step response of the closed-loop system. In HDDs, reading/writing of data is allowed once the head is safely placed within the range of $\pm 5\%$ of the track-pitch from the center of the track. We showed this error limit in all the plots showing displacement.

4.1. Simulation results

Simulated step response of the closed-loop system, including both VCM and PZT responses, is shown in Fig. 11 for a command of 1 μm displacement. Corresponding control signals are shown in Fig. 12. The dual actuator responds much faster than the coarse single actuator. The bandwidth of the VCM loop cannot be extended much further due to the presence of lightly damped resonant modes. The dual-stage actuator takes the advantage of the fast response of micro-actuator and reduces significantly the time taken to move the read–write head to the adjacent track. As the VCM actuator reaches near the target, the micro-actuator is brought back to the center of its operational range. The micro-actuator is therefore placed optimally for disturbance rejection during track following.

One of the key issues in using mass-produced PZT micro-actuator is the variation in resonant characteristics. The designed controller should be robust enough to accommodate such variations. Step responses were simulated with 20% variations in the resonant frequency of the PZT actuator to verify the robustness of the designed controller. The differences between these responses (Fig. 13) are insignificant.

Response is also simulated for step command of large displacement (50 μm) to study the effect of micro-actuator saturation on the performance (Figs. 14 and 15). In this case, the micro-actuator quickly saturates, and remains saturated until the coarse actuator brings the error sufficiently small for the micro-actuator to become actively involved again. The effect of input shaping FIR filter is clearly visible in the transient part of the micro-actuator response. It takes about 2.5 ms to bring the position error within the 5% tolerance band.

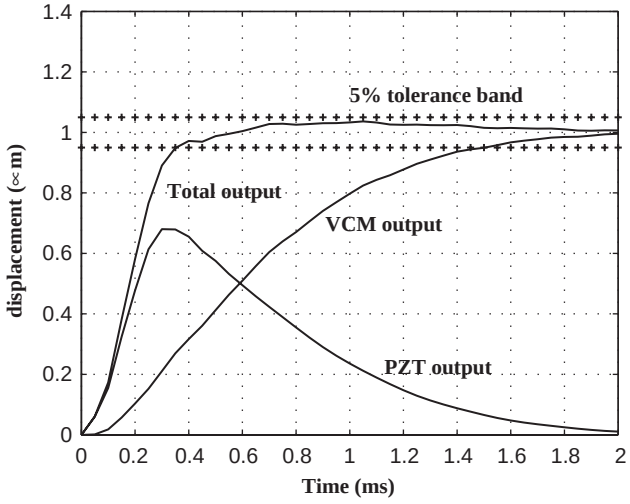

Fig. 11. Response for small step command: displacement.

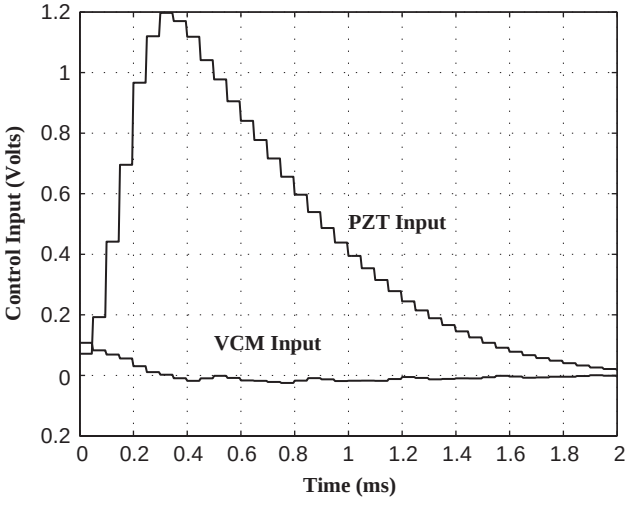

Fig. 12. Response for small step command: control inputs.

4.2. Implementation results

We implement the controller for the actuator of a 3.5 in HDD using the experimental setup described in Section 2.2. The response of the closed-loop system for a step change at the reference input is shown in Fig. 16.

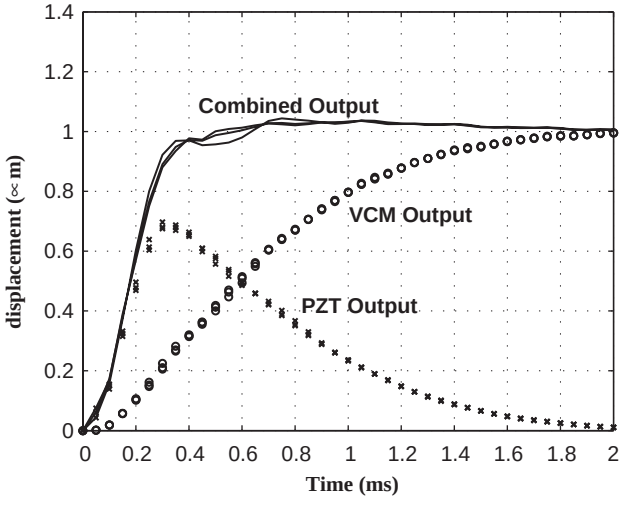

Fig. 13. Step response with 20% variation in PZT resonance frequency.

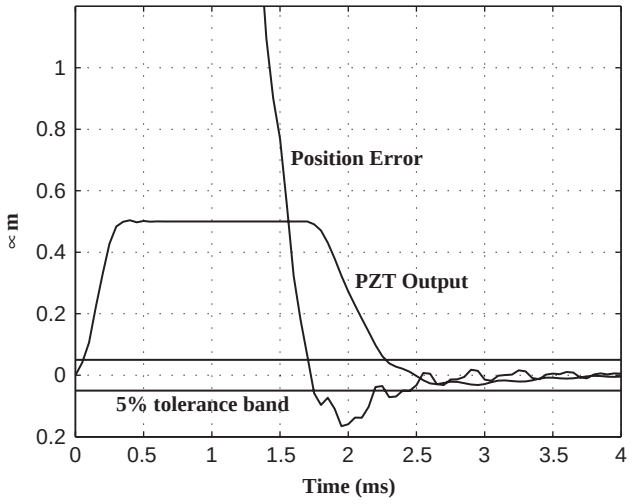

Fig. 14. Response for large step command: displacement.

The output of the micro-actuator is estimated and used to find the displacement of the VCM actuator, as described in Section 3.1. These estimated signals are also shown in Fig. 16. Input signals for VCM and PZT actuators are shown in Figs. 17 and 18, respectively. Implementation result conforms with that found through simulation. Performance for larger commands could not be verified due to the limitation of the feedback mechanism used in the experiments reported in this paper. The LDV uses the laser beam reflected from the read–write head slider to measure its velocity and displacement. Since the actuator moves on an arc, the reflected beam gets deviated from the line of incidence for longer displacement causing the LDV to be out of focus.

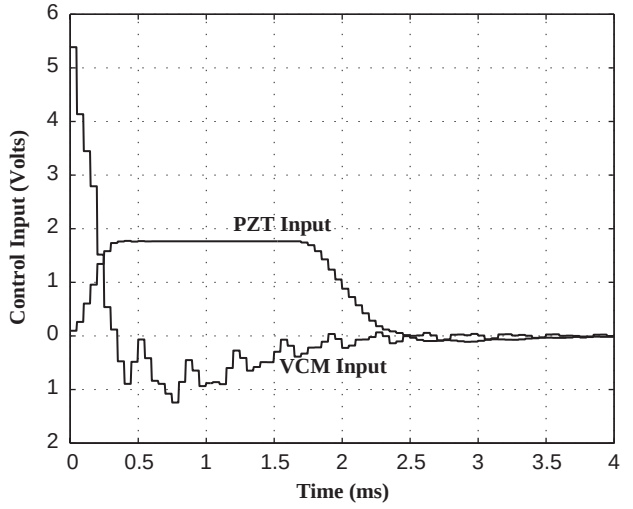

Fig. 15. Response for large step command: control inputs.

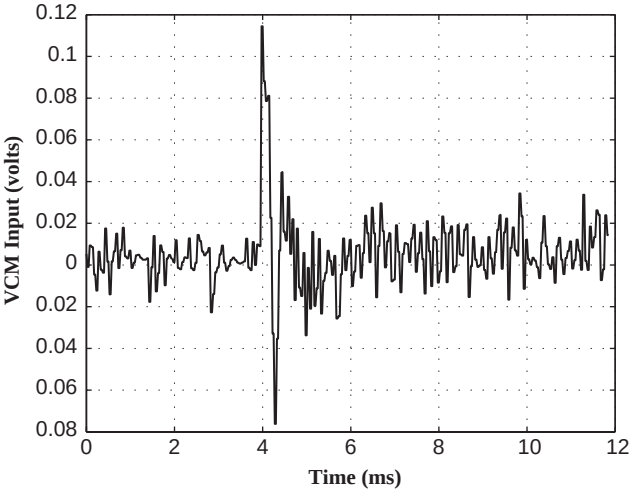

Fig. 17. Implementation results: VCM input.

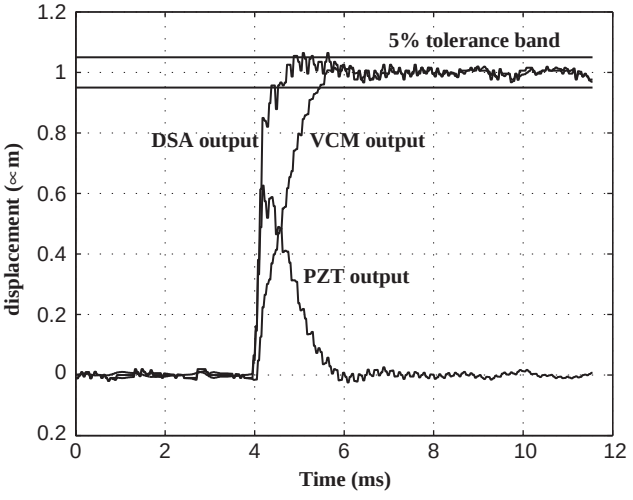

Fig. 16. Implementation results: displacement.

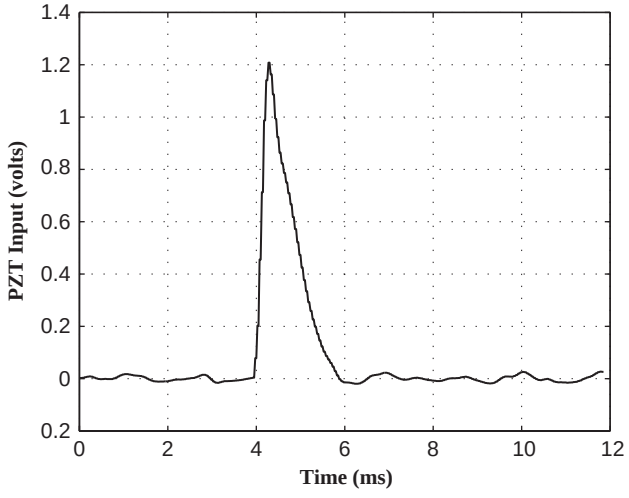

Fig. 18. Implementation results: PZT input.

5. Conclusion

We describe the linear model of a dual-actuated servomechanism used in hard disk drive. The controllers for the primary and secondary actuators are designed independently ensuring the stability of the VCM loop in the event of secondary-stage failure. Our design is based on exploiting the PZT micro-actuator to near its bandwidth capacity, by using a robust feedforward compensator. A PD compensator using observed state controls the slower VCM actuator. Only the states of the coarse actuator are estimated using the observer. Since the displacement of the VCM alone is not available for measurement, feedforward estimation of the micro-actuator's position is used to derive position of the slower actuator. This provides a reasonable compromise between accurate position tracking and fast transient acquisition of the read/write head's position. The overall improvement in performance achieved by the dual actuator configuration over the single actuator design is significant.

As can be observed, no real controller optimization has been performed, but rather classical design techniques have been applied. Contribution of this paper lies in the design philosophy of this dual-actuator problem. A complete design validation will have to involve a more realistic experiment including a study of the disturbance rejection for spindle motor vibration and eccentricity induced disturbances. At this point in time, given the achieved bandwidth, we are convinced that disturbances of upto 500 Hz can be adequately rejected.

We plan to further extend this design approach for a multi-rate servosystem using dual-stage actuator. A lower update frequency can be used for the VCM input. The desired bandwidth for the VCM can be kept low, and therefore 10 kHz sampling of the position signal should be sufficient. The fast responding micro-actuator, however, demands for sampling rate higher than 10 kHz. The feedforward compensator for the PZT actuator can be designed and implemented at higher sampling using interpolated information from the slower VCM system. Future work is also planned for analysis of robustness in presence of model uncertainty. Variation of the resonant frequency is very common issue in mass-produced PZT micro-actuators. The designed controller must be robust to accommodate such variations.

Acknowledgements

Iven Marels acknowledges the support from the National University of Singapore (NUS) for hosting him during his sabbatical leave in 2001. All authors express their sincere thanks to A/Prof. B.M. Chen for providing the laboratory facilities that made the experimental phase of this work feasible, and to the reviewers for their pertinent and helpful comments.

References

Ding, J., Tomizuka, M., & Numasato, H. (2000). Design and robustness analysis of dual stage servo design. Proceedings of the American control conference, Chicago, IL, USA.

Evans, R. B., Griesbach, J. S., & Messner, W. C. (1999). Piezoelectric micro actuator for dual stage control. *IEEE Transactions on Magnetics*, *35*(2), 977–982.

Franklin, G. F., Powell, J. D., & Workman, M. L. (1997). *Digital control of dynamic systems* (3rd ed.). Reading, MA: Addison-Wesley.

Grochowski, A., & Hoyt, R. (1996). Future trends in hard disk drives. *IEEE Transactions on Magnetics*, *32*, 185–1854.

Harnandez, D., Park, S. S., Horowitz, R., & Packard, A. K. (1999). Dual-stage tracking-following servo design for hard disk drive. *Proceedings of the American control conference*, San Diego, CA, USA (pp. 4116–4121).

Hirano, T., Fan, L. S., Lee, W. Y., Hong, J., Imaino, W., Pattanaik, S., Chan, S., Webb, P., Horowitz, R., Aggarwal, S., & Horsley, D. A. (1998). High bandwidth high accuracy rotary micro-actuators for magnetic hard disk drive tracking servos. *IEEE/ASME Transactions on Mechatronics*, *3*, 156–165.

Horsley, D. A., Harnandez, D., Horowitz, R., Packard, A. K., Pisano, A. P. (1998). Closed loop control of a microfabricated actuator for dual stage hard disk drive servo systems. *Proceedings of the American control conference*, Philadelphia, USA.

Hu, X., Guo, W., Huang, T., & Chen, B. M. (1999). Discrete-time LQG/LTR dual stage controller design and implementation for high tracking density HDDs. *Proceedings of the American control conference*, San Diego, CA, USA (pp. 4111–4115).

Kobayashi, M., Yamaguchi, T., & Horowitz, R. (2000). Track-seeking controller design for dual-stage actuator in magnetic disk drives. *Proceedings of the American control conference*, Chicago, USA (pp. 2610–2614).

Kollar, I. (1994). *Frequency domain system identification toolbox for use with Matlab*. Natik, MA: The Mathworks Inc.

Lee, S. H., Kim, Y. H., & Baek, S. E. (2000). Modeling and control of a dual stage actuator for hard disk drive servo system. *Proceedings of the American control conference*, Chicago, IL, USA (pp. 4254–4258).

Lee, S. H., Kim, Y. H., & Chung, C. C. (2001). Dual-stage actuator disk drives for improved servo performance: Track follow, track seek, and settle. *IEEE Transactions on Magnetics*, *37*(4), 1887–1890.

Mamun, A. A., Lee, T. H., & Tay, G. H. (2001). Efficient position encoding in hard disk drives using dual frequency servo bursts. *The proceedings of the 27th annual conference of the IEEE industrial electronics society IECON'01*, Denver, CO, USA, November 29–December 04.

Morarai, M., & Zafriou, E. (1989). *Robust process control*. Englewood Cliffs, NJ: Prentice-Hall.

Numasato, H., & Tomizuka, M. (2001). Settling control and performance of dual-actuator system for hard disk drives. *Proceedings of the American control conference*, Arlington, VA, USA (pp. 2779–2785).

Pintelon, R., Guillaume, P., Rolain, Y., Schoukens, J., & Vanhamme, H. (1994). Parametric identification of transfer function in the frequency domain—a survey. *IEEE Transactions on Automatic Control*, *39*, 2245–2260.

Schoukens, J., & Pintelon, R. (1991). *Identification of linear systems: A practical guideline to accurate modelling*. London: Pergamon Press.

Schroceck, S. J., & Messner, W. C. (2001). On compensator design for linear time-invariant dual-input single-output systems. *IEEE/ASME Transactions on Mechatronics*, *6*(1), 50–57.

Semba, T., et al. (1999). Dual-stage servo controller for HDD using MEMS microactuator. *IEEE Transaction Magnetics*, *35*(5), 2271–2273.

Singer, N.C. (1989). *Residual vibration reduction in computer controlled machines.* Technical Report 1030, MIT Artificial Intelligence Laboratory.

Suh, S. M., Chung, C. C., & Lee, S. H. (2001). Discrete-time LQG/LTR dual-stage controller design in magnetic disk drives. *IEEE Transactions on Magnetics*, *37*(4), 1891–1895.